NANO LETTERS

2009
Vol. 9, No. 3
984-988

Pressurized Liquid in Nanopores: A Modified Laplace-Young Equation

Yu Qiao

Department of Structural Engineering, University of California − San Diego, La Jolla, California 92093-0085

Ling Liu and Xi Chen*

Department of Civil Engineering and Engineering Mechanics, Columbia University, New York, New York 10027

Received October 3, 2008; Revised Manuscript Received December 26, 2008

ABSTRACT

In the current study, we analyze the motion of pressurized water molecules in nanopores of a well-crystallized, hydrophobic zeolite using both experiment and molecular dynamics simulation. It is discovered that, contradictory to the prediction of the classic Laplace-Young equation, the required infiltration pressure is highly dependent on the infiltration volume. A modified Laplace-Young equation is developed to take into consideration the effective solid−liquid interfacial tension, the thermal energy exchange, as well as the variation in configuration of confined liquid molecules. The last two factors are significant only when the nanopore diameter is comparable with the liquid molecule size. It is also remarkable that the infiltrated liquid molecules, when confined in the nanoenvironment, could transform from a single-chain conformation to a double-helical structure as the pressure increases, accompanied by an abrupt system free energy change that leads to different pressure-induced transport behaviors.

Understanding nanofluidic behaviors is of great scientific interest and immense technological importance. A large number of experimental and computational studies have been carried out,[1,2] shedding much light on fundamental mechanisms and processes of liquid, gas, and solid interactions in confining nanoenvironment, which underpin the development of advanced techniques of drug delivery, catalysis, separation and purification, energy conversion, nanofabrication, and so forth.[3,4] For example, by applying an external pressure, liquids can be forced into hydrophobic nanopores, nanochannels, or nanotubes, which provide an additional degree of freedom for system control and morphology adjustment.[5,6]

In a macroscopic channel, the behavior of a pressurized liquid can be described by the classic Poiseuille flow[7]

$$\bar{V} = \frac{D^2}{32\mu}\delta p \tag{1}$$

where $\bar{V}$ is the average flow rate, D is the channel diameter, μ is the liquid viscosity, and δp is the pressure gradient. For a microscopic channel, such as in a microreactor, the capillary effect must be taken into account. The equilibrium is given by the well-known Laplace-Young equation[8]

$$p_{\text{in}} = \frac{4\Delta\gamma}{D} \tag{2}$$

where $\Delta\gamma$ is excess solid−liquid interfacial tension and p_{in} is the pressure difference across liquid−gas interface at the onset of liquid infiltration, referred to as the infiltration pressure.

As the effective channel diameter approaches the liquid molecular size, the continuum theory may break down. The confined nanofluid is dominated by the interface characteristics. Extensive molecular dynamics (MD) simulations have been carried out on the unique molecular structures and transport behaviors of water inside nanotubes[9−13] and nanoporous materials.[14,15] It was found that water molecules may form a quasi-one-dimensional structure when confined by a nanotube.[16,17] Hummer et al.[18] reported that at a finite temperature an initially empty short carbon nanotube (with both ends open) can be filled instantaneously by surrounding water molecules. Such water infiltration behavior often leads to the conclusion that the tube inner wall is "frictionless",[12,19] which was supported by testing data.[20−22] However, most previous studies focused on spontaneous transport of water molecules under ambient conditions. The investigation on pressure-driven infiltration of liquids in nanochannels is still at its early stage. In operations of molecular sieves,[23] nanopipettes,[24] energy absorption systems,[25,26] and active control systems,[27] external pressures are often applied to force

* To whom correspondence should be addressed. E-mail: xichen@civil.columbia.edu.

10.1021/nl8030136 CCC: $40.75
Published on Web 01/30/2009

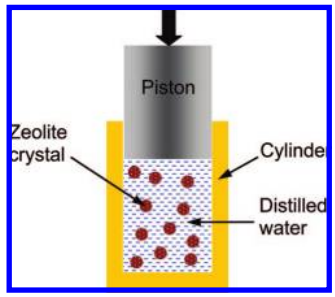

Figure 1. Schematic of the experimental setup.

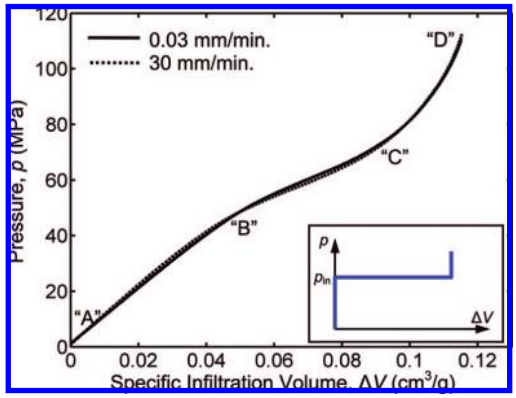

Figure 2. Typical water sorption curves of the hydrophobic zeolite at different loading rates. The insert depicts the prediction of the classic Laplace-Young equation.

liquids into nanoenvironment. The lack of understanding of the properties of pressurized liquid has imposed tremendous challenges to developing high-performance devices.

In the current study, we investigated a Zeolyst mobile-five-I (MFI) zeolite. The silica/alumina ratio was 280 and thus the nanopore surfaces were hydrophobic,[28] which was verified by using a Micromeritics ASAP-2000 Gas Absorption Analyzer. According to its crystal structure, the surface-to-surface pore diameter was 0.83 nm. The nanoporous structure/size was confirmed to be highly regular through an X-ray diffraction analysis.[29] The zeolite crystals were first dried in vacuum at 150 °C for 12 h and then treated in a nitrogen flow with silicon tetrachloride vapor at 400 °C for 1 h. After furnace cooling and thorough rinsing with deionized water, the material was hydrothermally treated in saturated water steam at 600 °C for 24 h, followed by vacuum drying at 120 °C for 12 h. The treated zeolite crystals were dispersed in distilled water and sealed in a stainless steel cylinder by a steel piston (Figure 1). The cross-sectional area of the piston was 286 mm^2. The piston was driven into the cylinder with the loading rate ranging from 0.03 to 30 mm/min. Typical sorption curves are shown in Figure 2, where the specific infiltration volume, ΔV, was taken as the difference between the piston intrusion volumes of the testing sample and a reference system that contained only distilled water, normalized by the mass of zeolite, $m = 0.512$ g. The corresponding temperature change at the center of the cylinder was measured by a type-E thermocouple insulated in a polyurethane cell (Table 1). The heat capacity of the water-zeolite suspension, C, was measured as 3.4 J/g•K through a differential scanning calorimetry analysis.

Table 1. The Results of the Calometric Measurement[a]

	temperature (°C)			
loading rate (mm/min)	A	B	C	D
0.1	20.8	21.2	21.6	21.6
1.0	20.7	21.1	21.6	21.7
10	20.7	21.2	21.7	21.6

[a] As shown in Figure 2, A indicates the onset of loading; B indicates the beginning of the secondary infiltration plateau; C indicates the end of the infiltration plateau; and D indicates the peak loading.

Since the nanopore surfaces are hydrophobic and the nanopore size distribution is uniform, according to eq 2, when the pressure p is relatively low, no infiltration should take place, as shown in the insert of Figure 2. Shortly after the external pressure is applied, infiltration begins, suggesting that the value of infiltration pressure (p_{in}) is quite small. From Figure 2, it can be seen that when the loading rate largely changes by 3 orders of magnitude, the variation in sorption isotherm curves is negligible. When the loading rate is 0.03 mm/min, the infiltration is completed in about 400 s. Since the zeolite crystal size is 5−10 μm, the average infiltration rate can be assessed as about 10 nm/sec. As the loading rate is increased to 30 mm/min, the nominal infiltration rate becomes 10 μm/sec. When the loading rate is relatively high, the infiltration process cannot be regarded as quasi-static, since according to the Poiseuille flow solution (eq 1) the variation in δp should be significant as $\bar{V}$ changes. The insensitivity of the sorption isotherm curves to the infiltration rate, together with the presence of the secondary infiltration plateau (BC) that will be discussed below, indicates that the confined liquid behavior does not follow the continuum theory.

Once the infiltration starts to take place, the measured sorption isotherm curves also conflict with the prediction of the Laplace-Young equation. As the infiltration volume increases, the pressure rises somewhat linearly, until p reaches about 60 MPa, where a secondary infiltration plateau is formed and ΔV increases more rapidly with the increase of p. Eventually, when the nanopores are filled, the system compressibility is lost and the slope of sorption curve tends to infinity. That is, once the infiltration starts, the nanopore size is not the only factor that affects the required pressure; otherwise the sorption curve would be flat (insert of Figure 2).

The calometric measurement results shown in Table 1 indicate that the liquid infiltration is an exothermic process. The system temperature increases with the infiltration volume (from A to C) and when the infiltration is completed the temperature variation stops (from C to D). The temperature change is insensitive to the large variation of the loading rate, which again is contradictory to the continuum theory that more work needs to be done to maintain a higher flow rate of a viscous liquid (eq 1).

In order to understand the experimental observation, a MD simulation was performed by using COMPASS force field.[30] A straight silicon dioxide nanochannel (Figure 3a) of a surface-to-surface diameter (distance between two opposite oxygen atoms) $D_0 = 0.83$ nm was employed as a close analogue to the MFI zeolite nanopore. One end of the

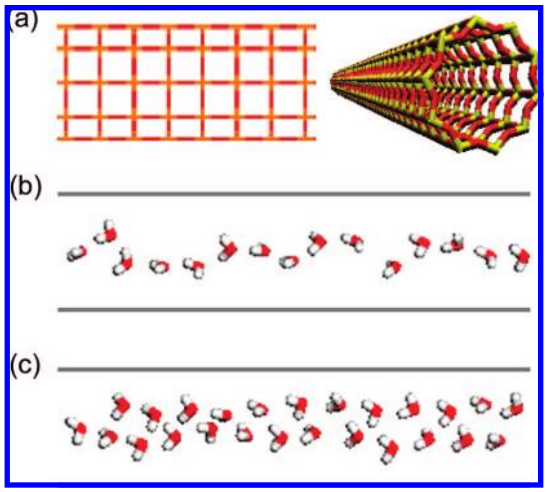

Figure 3. Snapshots of the MD simulation of pressure-driven infiltration at different loading steps. (a) A model nanochannel. (b) The formation of the single-chain structure of infiltrated water molecules (p = 50 MPa). (c) The formation of the double-chain structure of infiltrated water molecules (p = 125 MPa).

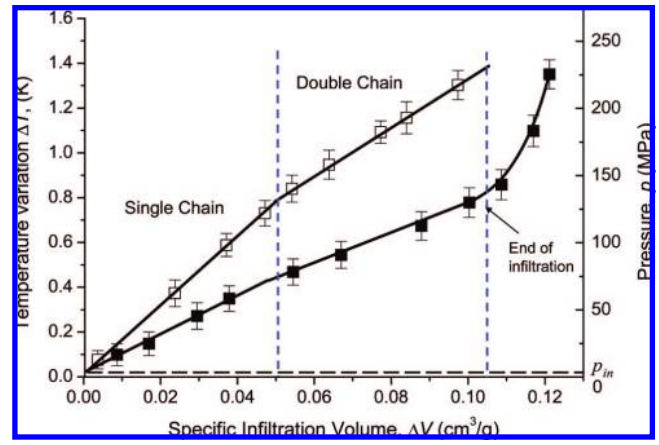

Figure 4. The MD simulation results of the pressure, p (solid symbol), and the temperature variation, ΔT (open symbol), as functions of the specific infiltration volume, ΔV.

nanochannel was closed, providing a simplified boundary condition for the symmetric compression of liquid from both ends of a long nanopore. During simulation, the nanotube was immersed into a 45 Å × 45 Å × 200Å reservoir bound by two rigid planes in the axial direction with periodical boundary conditions in the transverse directions. Initially, the reservoir was filled with water molecules with the density being maintained at 1 atm and 300 K. The liquid-to-nanopore mass ratio is set to be the same with the experiment. By moving the reservoir boundary axially, the pressure of water was varied. The effective pressure was computed from the state function of water. The redistribution of water molecules with pressure variation reflects the adiabatic pressure-driven infiltration. Note that the area accessible to the infiltrated molecules is smaller than that enclosed by the solid wall, primarily due to the van der Waals interaction, and thus the effective diameter of the liquid segment, D, is defined as $(D_0 + D_1)/2$, where D_1 is the diameter of the ring formed by the O atoms in the outmost layer of infiltrated water molecules. For the present MFI zeolite D = 0.6 nm.

With a rising p, the potential energy of liquid in reservoir is increased until the molecules are capable of overcoming the energy barrier to enter the tube. The energy barrier includes two components. First, on average each water molecule loses two hydrogen bonds when it enters the tube[18] and thus it could reorganize into a quasi-one-dimensional column; the change of free energy of the infiltrated molecules (with respect to the bulk phase) is ΔE. Second, the infiltrated liquid molecules are subjected to van der Waals and electrostatic interactions with nanopore atoms, and this term is denoted as U. The summation of $\Delta E + U$ is the total energy difference before and after infiltration, and when it is normalized by the lateral surface area of occupied nanochannel, it gives the effective excess solid−liquid interfacial tension, $\Delta\gamma$.[31] For the current system, ΔE and U per unit lateral area were calculated as 117.10 and −116.86 (Cal/mol)/Å^2, respectively, and thus $\Delta\gamma$ = 0.24 (Cal/mol)/Å^2, indicating that the nanochannel was hydrophobic. Note that the effect of nanopore curvature has been incorporated in the calculation of ΔE and U, and thus the reported value of $\Delta\gamma$ is valid only for the current pore geometry. According to eq 2, the infiltration pressure, p_{in}, should be 1.11 MPa, which matches well with the pressure at the onset of infiltration in the MD simulation (Figure 4) and is in qualitative agreement with the experiment observation, which supports the definition of the effective nanopore diameter of D discussed above.

At moderate pressure levels, Figure 3b shows the configuration of infiltrated water molecules, which form a helical water chain, compatible with the simulations of water conduction in carbon nanotubes of similar radii.[18] Before the water chain encountered the capped end, the infiltrated segment continuously grows along the axial direction. After the water segment reached the end with continued increase of p, starting from the pore opening the water molecules in the original helical chain move along the radial direction so as to one-by-one accommodate the newly infiltrated water molecules, and such "dislocation-like" propagation finally leads to the formation of a second helical water chain so as to alleviate the high potential energy (Figure 3c). Figure 4 shows p as a function of ΔV computed from the MD simulation, where the infiltrated water volume is normalized by a weighted mass of nanochannel to account for the geometrical difference between the straight pore used in simulation and the MFI zeolite in the experiment. It is readily seen that p increases almost linearly with ΔV after the infiltration has occurred, which implies that the continued infiltration has to overcome not only the initial energy barrier (characterized by p_{in}) but also a certain resistance that varies with the infiltration volume. The latter will be referred to as column resistance in the following discussion. After the double-helical structure is formed, the column resistance is reduced slightly; that is, the first water chain could ease the entrance of the molecules in the second chain. This two-staged characteristic of sorption curve fits with the experimental data quite well. With L denoted as the infiltrated length, the additional resistance can be stated as ηL, where η is the resistance per unit lateral surface area. When D is

large, the resistance that arises from the boundary layer can be neglected; for the nanopore under investigation, η is prominent, and therefore an additional pressure, Δp, is required. At steady-state

$$\Delta p = 4\eta L/D \tag{3}$$

By combining p_{in} and Δp, the total required pressure becomes

$$p = \frac{4(\Delta\gamma + \eta L)}{D} \tag{4}$$

The column resistance is offered by solid atoms to the water molecules sliding against them. In a nanopore with the diameter comparable with the liquid molecular size, all water molecules are exposed to the solid surface, whose resistance is proportional to its effective length. There are two ways of calibrating the resistance parameter (η) of the present system. First, directly from the fitting of the slope of the infiltration test $p-\Delta V$ curve in Figure 4, η was computed as 3.09 MPa according to eq 3. In the second method (which serves as an independent verification), an independent deceleration test was carried out for the same nanochannel and a single-chain water segment composed of 50 molecules. An initial axial velocity was assigned to this segment, and if the column resistance η plays an important role, the segment would be continuously decelerated and the resistance force could be estimated from the deceleration rate. On the basis of the velocity history of the mass center of the water molecules and from a large amount of simulations, η was computed to be 5.58 ± 0.4 MPa, which qualitatively agrees with that fitted from the infiltration test. Thus, we confirm that in such a small nanopore, the column resistance, η, could prominently affect the nanofluidic behaviors (for both transport and pressurized infiltration). Therefore, in the study on the motion of pressurized liquid in nanoenvironment, the Laplace-Young equation must be modified as eq 4, especially when the pore size is smaller than a few nanometers where the no-slip boundary condition is no longer valid; otherwise the column resistance would be independent of the infiltration depth. Here we show that such column resistance is important for the continued transport of liquid molecules in hydrophobic nanopores, and the principles can be extended to other types of nanotubes and nanochannels.[32,33]

The kinetic energy dissipated by the resistance is converted into the thermal vibration of the tube lattice and the kinetic energy of the water molecules, thereby increasing the system temperature (Table 1). As shown in Figure 4, the reservoir temperature computed from MD also increases almost linearly with ΔV and the increasing rate is slowed down during the second stage of infiltration. At the end of the infiltration process, the temperature is raised by about 1.3 K, comparable with the testing results. Here, the temperature variations can be directly compared because simulation uses the same liquid-to-nanopore mass ratio as experiment. Because the solid−liquid interaction is determined by the potential functions and is quite insensitive to the motion of water molecules, the temperature variation as well as the column resistance is independent of the infiltration rate.

During the pressure-induced infiltration, the mechanical work done to the system, W_M, is converted to two different parts: the interface energy, W_{in}, and the thermal energy, W_t. The first part corresponds to the area below the p_{in} line in Figure 4, which increases linearly with the infiltrated water volume. The second part is for overcoming the column resistance and is dissipated as thermal energy. In Figure 4, W_t is denoted by the area above the p_{in} line and below the $p-\Delta V$ curve. Ideally, if all the work done to overcome the column resistance W_t is dissipated as thermal energy with $\Delta TC = W_t$, one could estimate the temperature increase by the end of infiltration process as $\Delta T = 1.1$ K, which is at the same order of magnitude of Figure 4.

In summary, in a nanopore with the diameter comparable with the liquid molecule size, most of the infiltrated water molecules are in direct contact with the solid surface, which causes a significant resistance to their motion.[34] With a constant infiltration rate, a part of the external work is converted to the effective solid−liquid interfacial tension, which can be captured by the classic Laplace-Young equation. The rest of work is dissipated as heat, overcoming the energy barrier of solid atoms. The second part increases with the infiltration volume, and therefore the infiltration pressure is no longer a system constant. In the MFI zeolite under investigation, both experiment and simulation results show that the second part is dominant, which must be taken into consideration in studies on pressurized nanofluidics. A modified Laplace-Young equation is developed to account for both of the mechanisms. It is also discovered that when the applied pressure is relatively high, the single-chain structure of confined water molecules is no longer stable; a double-helical structure can be more energetically favorable. Such conformational changes could perturb the energy barrier related with pressure-induced transport of water molecules, and cause a different dissipation rate.

Acknowledgment. The work was supported by ARO under Grant W911NF-05-1-0288, NSF and Sandia National Laboratory under Grant CMMI-0623973, and NSF under Grant CMMI-0643726.

References

(1) Hu, G.; Li, D. *Chem. Eng. Sci.* **2007**, *62*, 3443–3454.
(2) Eijkel, J. C. T.; van den Berg, A. *Lab Chip* **2005**, *5*, 1202–1209.
(3) Stein, D.; Heyden, F. H. J. v. d.; Koopmans, W. J. A.; Dekker, C. *Proc. Natl. Acad. Sci. U.S.A.* **2006**, *103*, 15853–15858.
(4) Leary, S. P.; Liu, C. Y.; L.J., A. M. *Neurosurgery* **2006**, *58*, 805–823.
(5) Eroshenko, V.; Regis, R.; Soulard, M.; Patarin, J. *J. Am. Chem. Soc.* **2001**, *123*, 8129–8130.
(6) Han, A.; Qiao, Y. *J. Am. Chem. Soc.* **2006**, *128*, 10348–10349.
(7) Mott, R. L. *Applied Fluid Mechanics*; Prentice Hall: New York, 2005.
(8) Ibach, H. *Physics of Surfaces and Interfaces*; Springer: New York, 2006.
(9) Huang, B.; Xia, Y.; Zhao, M.; Li, F.; Liu, X.; Ji, Y.; Song, C. *J. Chem. Phys.* **2005**, *122*, 84708.
(10) Qiao, Y.; Cao, G.; Chen, X. *J. Am. Chem. Soc.* **2007**, *129*, 2355–2359.
(11) Striolo, A. *Nano Lett.* **2006**, *6*, 633–639.
(12) Whitby, M.; Quirke, N. *Nat. Nanotechnol.* **2007**, *2*, 87–94.
(13) Liu, L.; Qiao, Y.; Chen, X. *Appl. Phys. Lett.* **2008**, *92*, 101927.
(14) Bougeard, D.; Smirnov, K. S. *Phys. Chem. Chem. Phys.* **2007**, *9* (2), 226–245.

(15) White, C.; Ruiz-Salvador, A. R.; Lewis, D. W. *Angew. Chem., Int. Ed.* **2004**, *43* (4), 469–472.
(16) Kolesnikov, A. I.; Zanotti, J.-M.; Loong, C.-K.; Thiyagarajan, P.; Moravsky, A. P.; Loutfy, R. O.; Burnham, C. J. *Phys. Rev. Lett.* **2004**, *93*, 035503.
(17) Mann, D. J.; Halls, M. D. *Phys. Rev. Lett.* **2003**, *90*, 195503.
(18) Hummer, G.; Rasalah, J. G.; Noworyta, J. P. *Nature* **2001**, *414*, 188–190.
(19) Supple, S.; Quirke, N. *Phys. Rev. Lett.* **2003**, *90*, 214501.
(20) Holt, J. K.; Park, H. G.; Wang, Y.; Stadermann, M.; Artyukhin, A. B.; Grigoropoulos, C. P.; Noy, A.; Bakajin, O. *Science* **2006**, *312*, 1034–1037.
(21) Sholl, D. S.; Johnson, J. K. *Science* **2006**, *312*, 1003–1004.
(22) Majumder, M.; Chopra, N.; Andrews, R.; Hinds, B. J. *Nature* **2005**, *438*, 44–44.
(23) Deamer, D. W.; Akeson, M. *Trends Biotechnol.* **2000**, *18*, 147–151.
(24) Hong, M. H.; Kim, K. H.; Bae, J.; Jhe, W. *Appl. Phys. Lett.* **2000**, *77*, 2604–2606.
(25) Chen, X.; Surani, F. B.; Kong, X.; Punyamurtula, V. K.; Qiao, Y. *Appl. Phys. Lett.* **2006**, *89*, 241918.
(26) Borman, V. D.; Crekhov, A. M.; Troyan, V. I. *J. Exp. Theor. Phys.* **2000**, *91*, 170–181.
(27) Kong, X.; Qiao, Y. *J. Appl. Phys.* **2006**, *100*, 014308.
(28) Jansen, J. C.; Stocker, M.; Weitkamp, J.; Karge, H. G. *Advanced Zeolite Science and Applications*; Elsevier Science: New York, 1994.
(29) van Koningsveld, H. *Compendium of Zeolite Framework Types*; Elsevier Science: New York, 2007.
(30) Sun, H.; Ren, P.; Fried, J. R. *Comp. Theor. Polym. Sci.* **1998**, *8*, 229–246.
(31) Gennes, P.-G. d.; Brochard-Wyart, F.; Quere, D. *Capillarity and Wetting Phenomena: Drops, Bubbles, Pearls, Waves*; Springer: New York, 2004.
(32) Cao, G.; Qiao, Y.; Zhou, Q.; Chen, X. *Phil. Mag. Lett.* **2008**, *88*, 371–378.
(33) Cao, G.; Qiao, Y.; Zhou, Q.; Chen, X. *Mol. Simul.* **2008**, *34*, 1267–1274.
(34) Chen, X.; Cao, G.; Han, A.; Punyamurtula, V. K.; Liu, L.; Culligan, P. J.; Kim, T.; Qiao, Y. *Nano Lett.* **2008**, *8*, 2988–2992.

NL8030136